

Article

Reactivation System for Proton-Exchange Membrane Fuel-Cells

Carlos Restrepo ^{1,*}, Oriol Avino ¹, Javier Calvente ¹, Alfonso Romero ¹, Miro Milanovic ² and Roberto Giral ¹

¹ Departament d'Enginyeria Electrònica, Elèctrica i Automàtica, Universitat Rovira i Virgili, Avda. Països Catalans 26, Campus Sescelades, Tarragona 43007, Spain; E-Mails: oriol.avino@urv.cat (O.A.); javier.calvente@urv.cat (J.C.); alfonso.romero@urv.cat (A.R.); roberto.giral@urv.cat (R.G.)

² Faculty of Electrical Engineering and Computer Sciences, University of Maribor, Smetanova ul. 17, 2000, Maribor, Slovenia; E-Mail: milanovic@uni-mb.si

* Author to whom correspondence should be addressed; E-Mail: carlos.restrepo@urv.cat; Tel.: +34-977-297-052; Fax: +34-977-559-605.

Received: 28 March 2012; in revised form: 27 June 2012 / Accepted: 9 July 2012 /

Published: 13 July 2012

Abstract: In recent years, Proton-Exchange Membrane Fuel Cells (PEMFCs) have been the focus of very intensive researches. Manufacturers of these alternative power sources propose a rejuvenation sequence after the FC has been operating at high power for a certain period of time. These rejuvenation methods could be not appropriate for the reactivation of the FC when it has been out of operation for a long period of time or after it has been repaired. Since the developed reactivation system monitors temperature, current, and the cell voltages of the stack, it could be also useful for the diagnostic and repairing processes. The limited number of published contributions suggests that systems developing reactivation techniques are an open research field. In this paper, an automated system for reactivating PEMFCs and results of experimental testing are presented.

Keywords: reactivation system; PEM fuel cell; automated system

1. Introduction

Power systems based on proton-exchange membrane fuel cell technology have been the object of increasing attention over recent years. This is because they appear very promising for both stationary

and mobile applications due to their high-efficiency, low-operating temperatures allowing fast start-up, high-power density, solid electrolytes, long cell and stack lives, low corrosion, and non-polluting emissions into the environment [1–3].

One of the areas addressed by researchers has been FC modelling. In the literature, there are several models that describe polymer electrolyte membrane fuel cell (PEMFC), ranging from static, dynamics, frequential, impedance spectroscopy, empirical, electrochemical, electrical circuit, artificial neural network, and real-time simulation models. In addition, models are also found in the literature that analyze and/or design air flow controllers to protect the FC from oxygen starvation during load transients, estimate the oxygen excess ratio, analyze the behavior of transient flooding in the cathode, permit studying of interactions between the different elements that can be connected to the FC, among many others [2–13]. The estimation of parameters by a specific FC model is also an area of interest for researchers as evidenced by the number of publications that can be found on this topic [13–15].

Another recent area attracting research is the design of power converters for being connected to the FC [13,16–26]. These power converters allow to manage in a safe and efficient manner the energy delivered by the stack, which is to be used over a wide-range of applications. The studies focus primarily on the design of DC/DC converters, inverters and filters with high-efficiency, reliability, low-ripple input currents, and isolated structures that ensure the correct and safe operation of the FC under all load conditions. The use of an FC emulator is the most suitable way of testing these power converters and other different devices before being connected to the FC. Advances in computing technologies, such as microprocessors, field-programmable gate arrays (FPGAs), digital signal controllers (DSP), multi-core processors and stream processors, have driven the development of increasingly complex, fast, versatile, and economical FC emulators into becoming another area of research. These, then, are needed in research, since they enable both power stages and control strategies to be evaluated, in a safe, economical, realistic, real-time and repetitive manner. In addition, different FC models and types can be studied using FC emulators [5,10,27–30]. The system formed by the emulator and the devices to be connected to the FC, known as hardware-in-the-loop (HIL), is one of more recently studied research areas [10,27,28,30].

The output characteristics of the PEMFC are limited by the mechanical devices that are used to maintain the air-flow in the cathode by means of a compressor-motor, regulate hydrogen-flow in the anode through an adjustable valve command, control the temperature using a cooling-fan, and adjust the humidity of the air in the cell by means of a humidity-exchanger. Hence, the time constants are dominated by a fuel delivery system. As a consequence, a load transient demand will cause a high-voltage drop after a short time, well-known as the oxygen starvation phenomena [31]. This operational condition is evidently harmful for the FC and for this reason the FC is considered as slow dynamic-response equipment with respect to the transient load's requirement. Therefore, batteries, ultracapacitors or other auxiliary power sources are needed to work together with the FC in order to ensure a fast response to any load power changes. Consequently, the systems formed by FC and other auxiliary power sources, known as FC hybrid systems, have been one of the more studied areas over recent years [21,22,32,33].

As mentioned above, oxygen starvation is a complicated phenomenon that reduces an FC's life. This phenomenon entails a rapid decrease in cell-voltage, which in severe cases can cause a hot spot, or even burn-through on a membrane's surface [3]. Therefore, in the literature it is possible to find many

studies on the oxygen starvation phenomenon, and it has become another area of research regarding FCs [5,8,25,34–37].

During shipping or idleness for a long period of time, the FC stack could lose its performance and it is necessary to reactivate it. The Nexa FC, manufactured by Ballard, has a rejuvenation sequence process that is performed prior to normal shutdown if the FC has been running for 10 to 30 min at an average gross stack power of 200 W or greater, measured over the last 10 min of operation [38]. This automated rejuvenation process lasts approximately 3 min and restores any FC stack performance that may have been degraded by certain contaminants, by repeatedly cycling stack voltage under the presence of internal parasitic loads. The drawback of the Nexa system is that a separate software has never been designated for the rejuvenation cycle and, depending on the severity of the performance degradation, the short duration of its rejuvenation process might be insufficient for obtaining the FC reactivation after a long inactivity period. Also, taking into account that the Nexa is a self-humidified closed system FC, triggering the Nexa's rejuvenation cycle with relatively high power levels without a previous reactivation cycle could endanger the FC. Additionally, not all FC's have the internal system of rejuvenation that Nexa has. Systems that achieve a rejuvenation of the FC stack can be found within two groups of patents, as described below. The performance of the stack may gradually decrease due to the accumulation of water in the stack, thus producing a blockage of those channels through which gases circulate. A technique that includes applying a vacuum to the manifold of a FC stack in order to remove at least some of the accumulated water is presented in [39]. The performance of FC can also be affected by impurities known as electrocatalyst poisons, either from the reactant streams or from within the FC as intermediate species generated during FC reactions, which may be absorbed or deposited on the surface of the anode, and the cathode electrocatalysts [40]. The patents [40–42] show a system for removing electrocatalyst poisons and obtaining an improvement in FC performance. All the processes described are used to rejuvenate a healthy FC but none can be applied for achieving reactivation of a long time stored or repaired FC. Some user guides [43] recommend manual activation procedures to ensure a progressive humidification of the stack while performing frequent voltage measurements on each of the stack cells to ensure that they are always above a safe value. This process is slow, wastes a lot of hydrogen, and is manpower intensive.

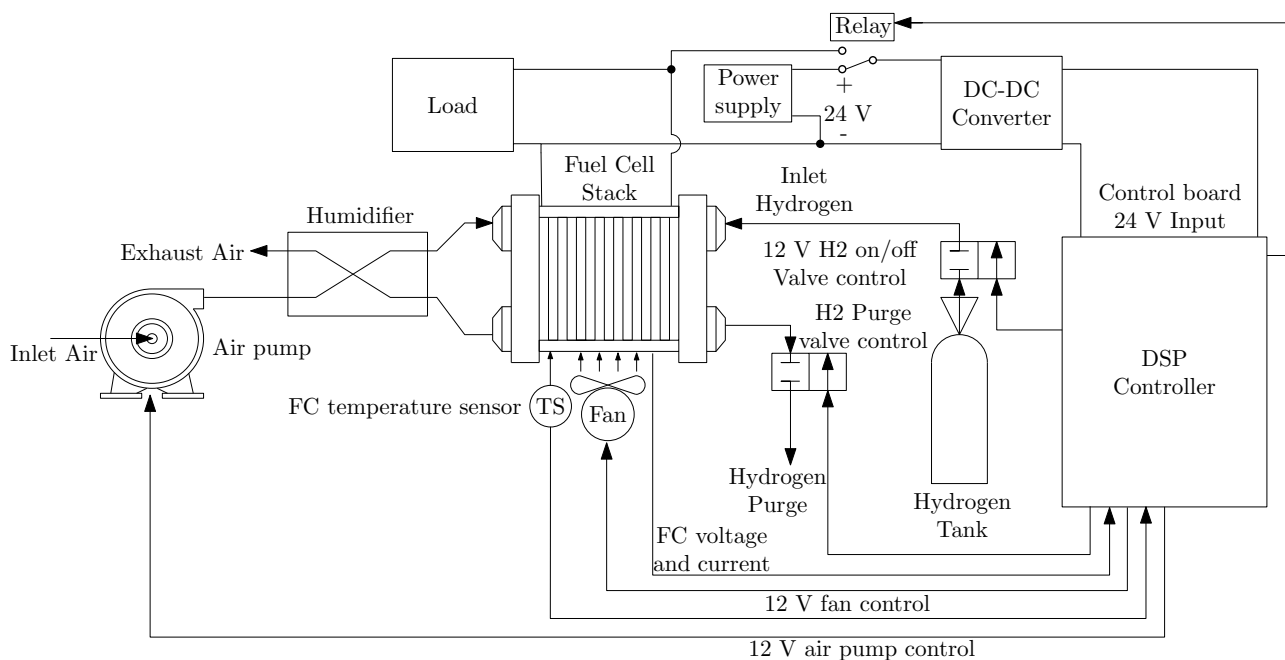
In addition to reducing the duration and the hydrogen consumption of the manual procedure, the proposed automated system implements a control of the fuel cell temperature. The regulation of the temperature and the simultaneous measurement of all the cell voltages are key factors to ensure a safe and quick reactivation procedure. The long, and tedious process of measuring manually the cell voltages requires the full attention of the operator, whose fatigue can result in a reactivation failure with damages to the fuel cell. Also a human operator can be slow to detect the alarm factors that, in the automated system, trigger almost instantaneously a safe shut-down response. The study of the technical literature on the different FC power electronics application research areas, which has been resumed previously, has shown that there is not any automated system that can perform the reactivation of a PEMFC. This means that an automated reactivation system, of which nothing has been published nor patented yet, using a combination of software and hardware can be of great interest. This work opens the door to the reactivation of fuel cells as a new area of research that will be vital to ensure a better positioning of PEMFCs as practical electrical generators and, together with other areas oriented towards improving

the fuel cell stack life-time, will be crucial to ensure a better placement of the power systems based on proton exchange membrane fuel cell (PEMFC) technology in both stationary and mobile applications.

The rest of this paper is organized as follows: Section 2 describes the PEMFC system to reactivate, and Section 3 performs a detailed description of the hardware and software that comprises the proposed reactivation system. Finally, the last two sections present respectively experimental results and the conclusions of this work.

2. Description of the PEMFC System to Reactivate

The air-cooled proton exchange membrane fuel-cell stack to be reactivated after several years of inactivity is the PC3F40 of the Palcan Fuel Cell Co. Ltd., which has 40 membrane electrode assemblies (MEA). The PC3F40 fuel-cell power model includes the stack, air pump, humidifier, valves, relay, DC-DC converter, digital-signal processing (DSP) controller and displays, as shown in Figure 1. The DSP-controller gets the feedback signals, such as fuel-cell voltage, current, and temperature, from the stack and sends the control signal to the air-pump, fan, valves and relay. The manufacturer recommends shutting-down the system immediately by turning the key to the off-position, if the following situations should occur: stack is over-heating, that is, the fuel cell temperature is over 75 °C, stack voltage is under 18 V, stack current is over 20 A, and the system connection is incorrect. In addition, the manufacturer delivers a list of warnings to be considered for obtaining good functioning of the fuel-cell. Many of these warnings are easy to perform, such as: never bring the inlets of air and hydrogen pressures be above 8 psig, never use pure oxygen in the stack, never use the stack when cooling air is not flowing along the cooling channels, or never use a stack without proper cooling. One of the warnings determines the optimal point of operation as: monitor the temperature at the core outlet and never let it be above 75 °C, the stack performs at its best between 50 °C and 65 °C. Finally, the last warning is a little more complex to perform as explained in the next session; this is: for better operation, a cell-voltage monitor is required, and never allow a cell to go below 0.45 V. Therefore, the manual reactivation procedure recommended by the manufacturer [43] requires that a human operators monitors the 40 voltages of the stack cells at each load change to perform an emergency shutdown if any of the voltages goes below the minimum safety level. Performing this task manually is slow and tedious and could easily result in a failure to detect a dangerous situation in one of the cells. Our own experience in this manual reactivation procedure is that two very motivated human researchers failed to detect the undervoltage situation which resulted in a cascade damage of several of the stack cells. When we detected the undervoltage and did the recommended emergency shut-down it was too late to save the cells. We strongly believe that an automated procedure providing faster and almost continuous voltage monitoring to shut-down the fuel cell much more quickly under the undervoltage detection should be mandatory. In addition, global undervoltage, overload and overtemperature dangerous levels can be avoided much more easily and quickly by an automated reactivation system.

Figure 1. Block diagram of the PC3F40 fuel cell system.

3. Description of the PEMFC Embedded and Automated Reactivation System

In the previous section, the main features of the PEMFC system considered for reactivation were described in detail. The complexity of the system to be reactivated, and the reactivation process itself, become crucial for the development of an embedded and automated reactivation system. The main functions of this system are: sensing the cells' voltages in the FC, sensing and controlling the temperature, sensing the current generated by the stack in order to determine the power-operation point, keeping the FC within the security conditions recommended by the manufacturer, and optionally allowing communication for the monitoring of key FC variables from an external system, such as a computer. This section presents the main characteristics of the hardware and software that constitute the PEMFC reactivation system.

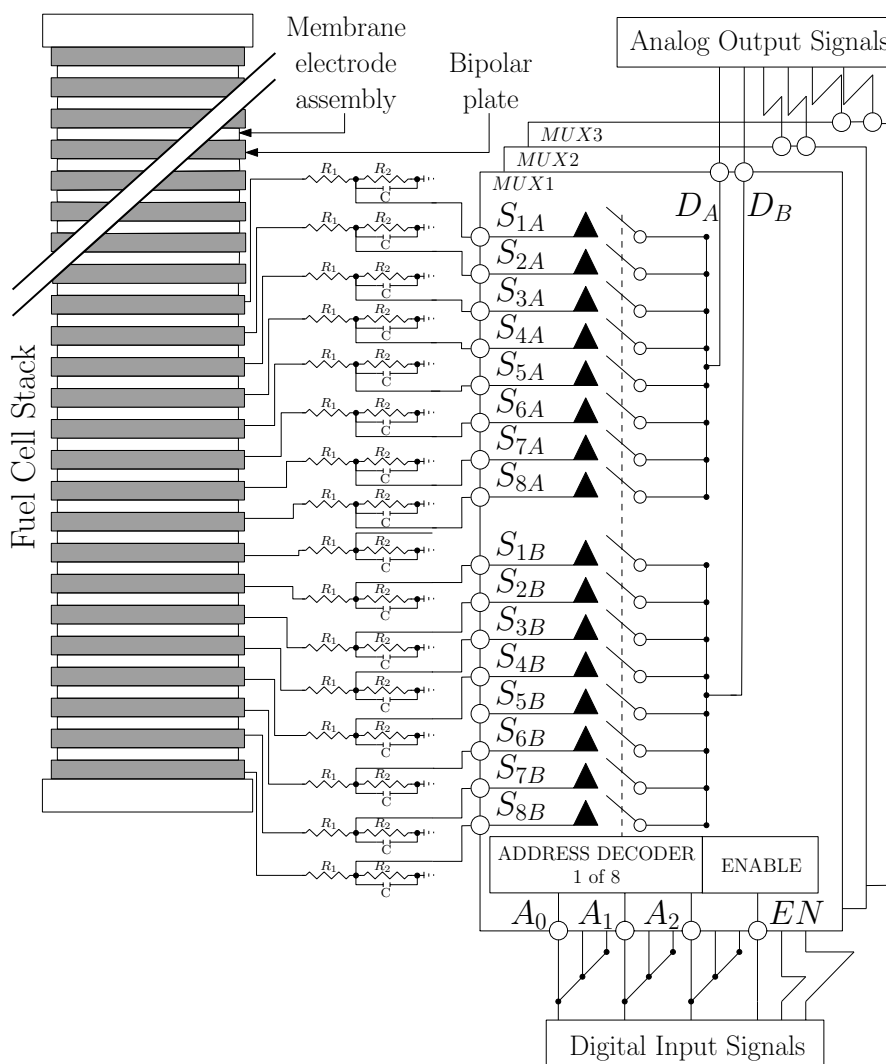
3.1. Hardware of the Fuel Cell Reactivation System

3.1.1. Cell-Voltage Sensing and Multiplexing Stage

In general, fuel cells are systems with a large number of cells in series, thus making monitoring of the cell-voltage a complex task. This difficulty is due to the need of a data acquisition (DAQ) stage with 40 differential analog input channels to monitor 40 cell voltages in the specific case of the PC3F40 FC of Palcan and 47 differential analog input channels, in the case where it is necessary to reactivate the Nexa FC of Ballard. Although the market offers a few cards with a large number of differential analog input channels, such as the NI USB-6255, the PXI-6255, the NI PXI-6225, and the NI PCI-6255 of National Instruments, the USB-AI12-128A of Acces I/O Products, the DaqLab/2000 and DaqScan/2000 series of the Measurement Computing Corporation, their high-cost is the main disadvantage for their use. Therefore, it is necessary to build a system for monitoring those voltages in a stack that can be

extended to other possible cells requiring reactivation. The sensing voltage cells system consists of precision resistive dividers, as illustrated in Figure 2, that convert the differential analog signals of the cells into referenced single-ended (RSE) signals, with a range of voltages of 0 V to 5 V, corresponding to the digital analog converter (DAC) range that will be used. The reading accuracy of the cell-voltages depends primarily on ADC resolution, the accuracies of the resistors, and the final voltage ranges of the resistive dividers. The manner in which the resistors are connected to the bipolar plates of the FC follows the standard RJ45 for the connectors and their wiring. A capacitor is placed at each output of the resistive divider in order to stabilize and filter the acquired signal, as shown in Figure 2. The acquired signals pass through a multiplexing stage, which converts up to 48 differential signals to be sensed into only 6 analog channels and requires 3 digital outputs for the address decoders of all the multiplexers ($k = (A_2A_1A_0) \in \{(000), (001), \dots, (111)\}$) and 3 digital outputs for enabling each of the multiplexers, as depicted in Figure 2. The main characteristics of the high-performance CMOS analog multiplexer DG407 Vishay Siliconix is its fast transition time of 200 ns. The solution for acquiring the differential voltage proposed in this work is simple, low-cost, and provides high-speed acquisition with good accuracy. The final implemented system senses all the voltage cells and the stack voltage, current and temperature every 200 ms, which is much faster than the monitoring provided by the manual procedure.

Figure 2. Circuit schematic of the multiplexing stage.



3.1.2. PWM FC Fan Driver Control and FC Current and Temperature Sensing Stage

Since the FC performs better between 50 °C and 65 °C, it is important to control the temperature of the stack to obtain a reactivation in less time, and thus ensure lower consumption of hydrogen during the procedure. This requires designing a stage that could control the FC fan using pulsed-width modulation (PWM) signals and also characterizing the FC temperature sensor. Figure 3 presents the circuit schematic of the stage responsible for the FC temperature control. The PWM fan motor driver is implemented using a totem-pole output and the positive voltage regulator L78XX is selected according to the voltage that is powering the fan, which is 12 V in the case of the PC3F40 FC. In order to allow operation with high currents, the IRFP150N MOSFET and the BYV79E diode are oversized. The FC thermistor is connected to a conditioning circuit that consists of a resistance divider with a precise 5 V voltage source, as shown in Figure 3. The thermistor was characterized for all the temperature ranges of the FC using the experimental setup detailed in Figure 4. The obtained FC thermistor characteristic is plotted in Figure 5. Using a curve-fitting toolbox, the MATLAB software adjusts the coefficients of the cubic polynomial of the thermistor resistance as a function of the temperature in °C as:

$$R_t(Temp) = -0.07108 \cdot Temp^3 + 16.37 \cdot Temp^2 - 1350 \cdot Temp + 4.186 \times 10^4 \quad (1)$$

Therefore, the FC temperature as a function of voltage obtained by the conditioning circuit V_{temp} , presented in Figure 3, is:

$$Temp(V_{temp}) = 1.914 \cdot V_{temp}^3 - 13.96 \cdot V_{temp}^2 + 54.04 \cdot V_{temp} - 38.74 \quad (2)$$

Figure 3. Circuit schematic of the PWM fan driver, current and temperature sensing of the PEMFC.

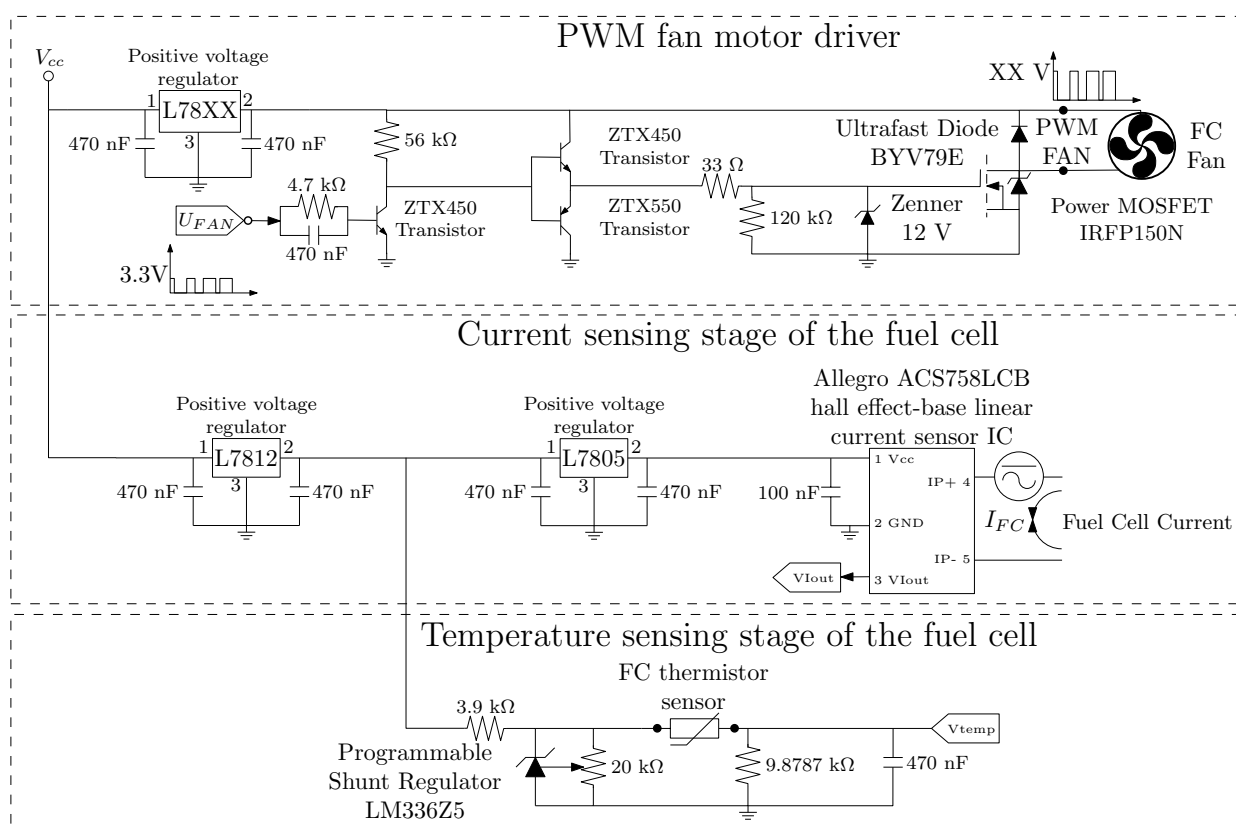


Figure 4. Experimental configuration to obtain the characteristic of the fuel cell thermistor: (a) QuadTech 1910 inductance analyzer used to accurately measure the resistance; (b) Fluke 179 digital multimeter to verify the measurement of temperature inside the oven; (c) Mytron’s KPK 35 oven; (d) thermistor under test.

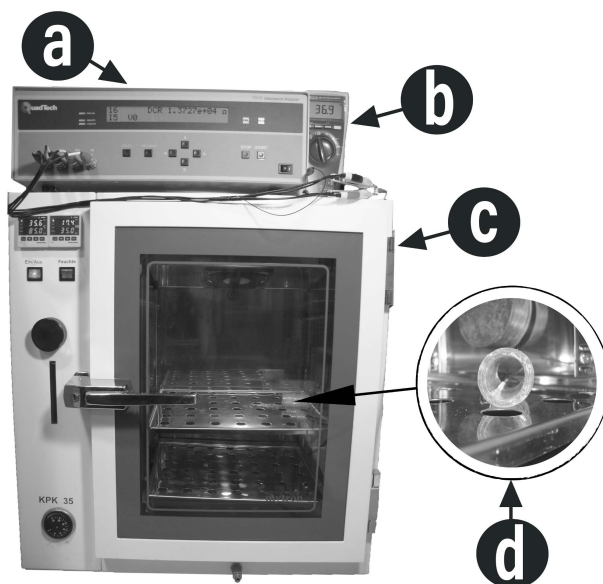
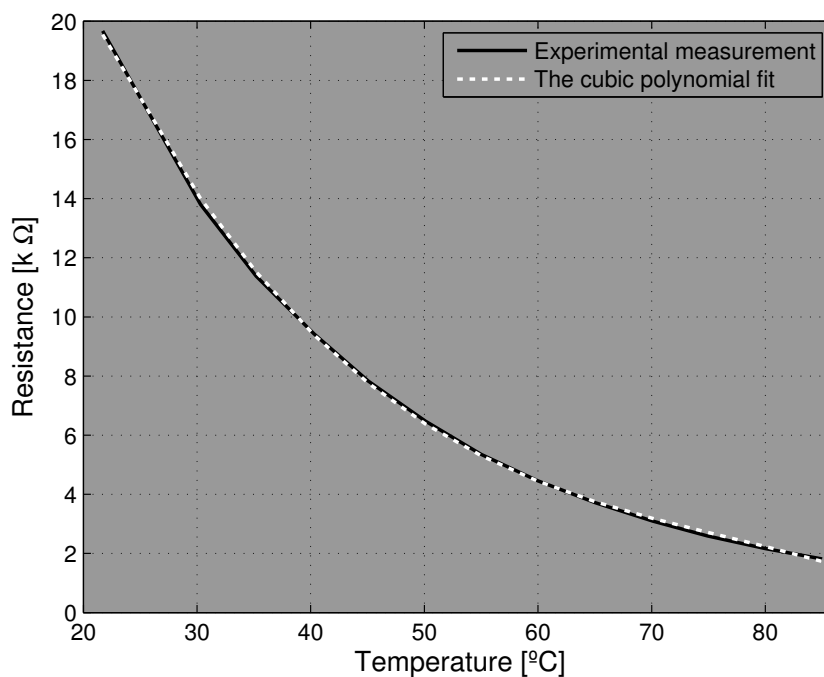


Figure 5. Fuel cell thermistor characteristic. In black line is depicted the experimental measurement using the configuration of Figure 4 and in white line is represented the cubic polynomial fit of Equation (1).



Finally, a current sensor is installed at this stage to measure the current generated by the cell, and thus determines its power output at all times. The used Allegro ACS758xCB Hall effect-based linear current sensor can measure currents up to 50 A, which allows its use with other kinds of FC's. Additionally, it has a sensitivity of 40 mV/A, with an internal resistance of only 100 $\mu\Omega$, thus providing a low-power loss.

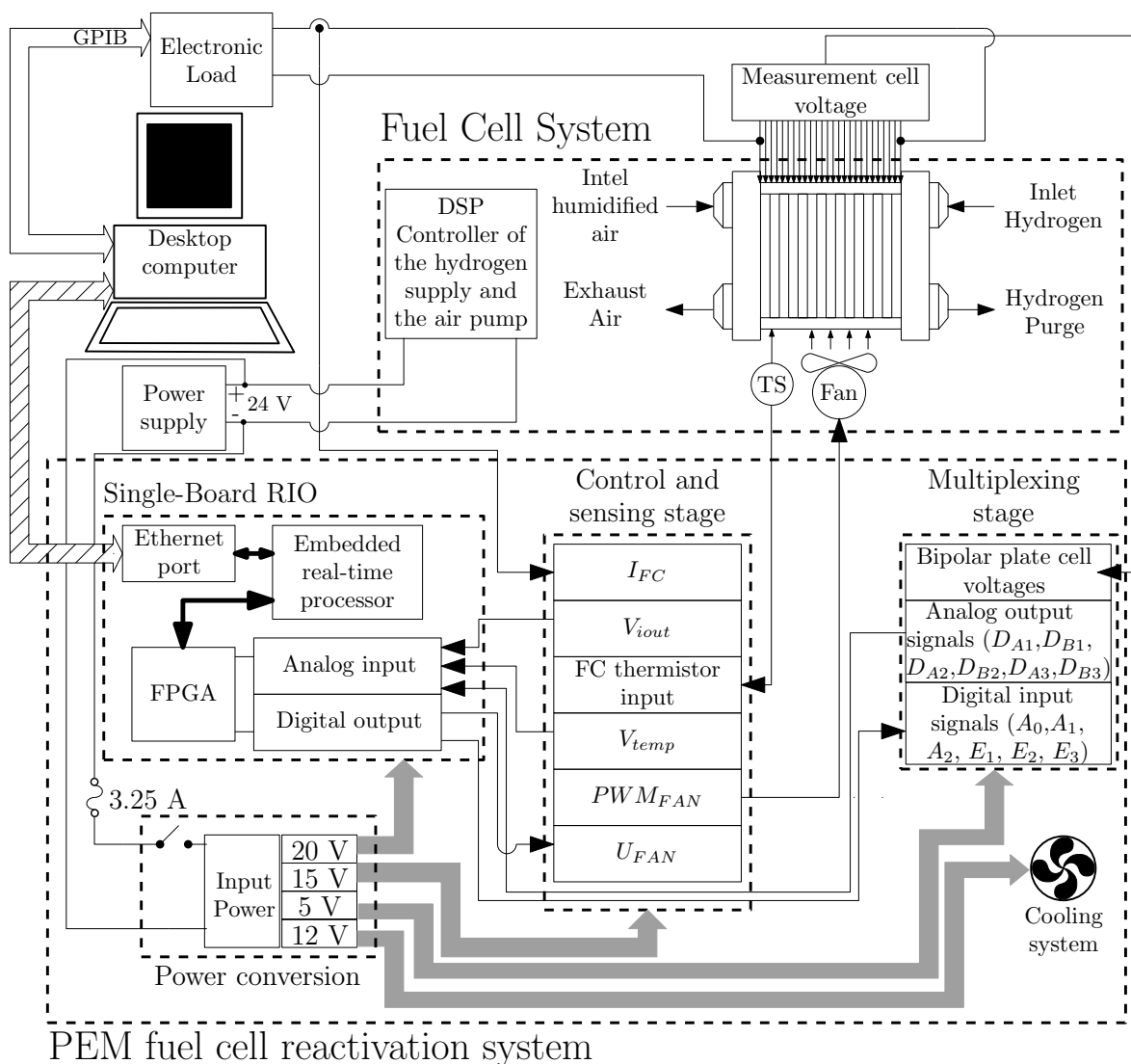
Regulating the stack temperature in a narrower optimal range than that originally provided by the fuel cell accelerates the reactivation procedure, in this way reducing the fuel consumption. Monitoring the temperature also provides the automated system with the capability of shutting down the fuel cell in case of an overtemperature situation.

3.1.3. Embedded Control System

The selected system for the management of the systems presented above is the NI Single-Board RIO sbRIO-9631, which is cost-optimized with an embedded real-time processor, reconfigurable FPGA, and analog and digital inputs/outputs on one printed circuit board (PCB) [44]. The open design decreases cost and provides flexibility for designing a customized enclosure. NI Single-Board RIO devices are designed for acquisition applications that require high performance and reliability.

3.1.4. PEM Fuel Cell Reactivation System

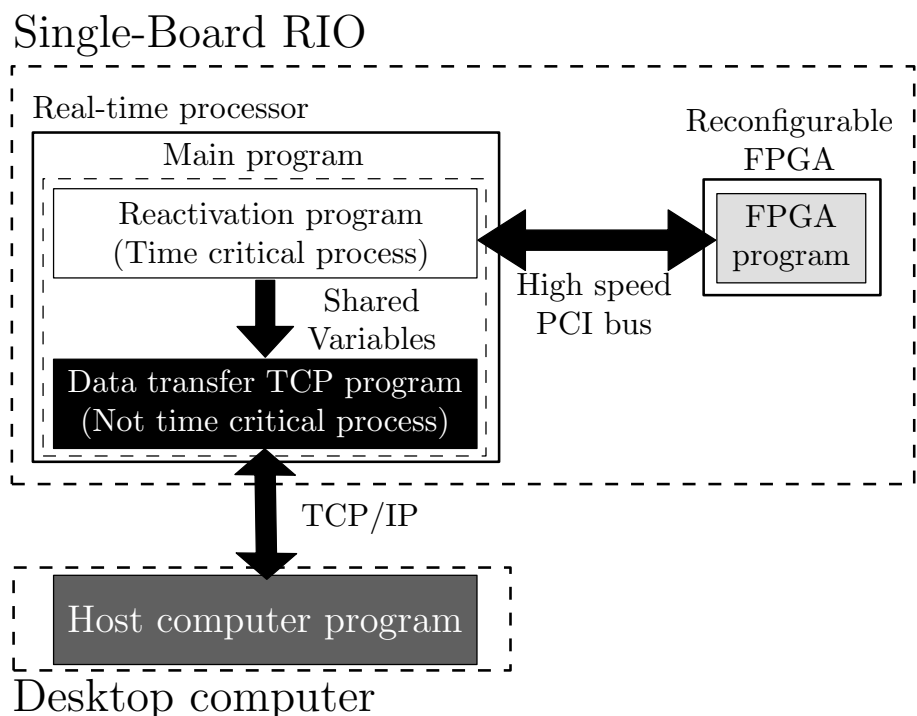
Figure 6 shows the configuration for all the hardware described above including the FC, the electronic load, and the computer for the monitoring and storage of the main variables. The difference in the FC system presented in Figure 6 with respect to the one described in Figure 1 is that the DSP does not control the temperature of the FC, but still controls the hydrogen supply and the air pump. It was necessary to design an additional stage of power conversion due to the different voltages of each stage comprising the reactivation system. The input voltage of this power conversion stage is the same power supply used by the FC control system, as shown in Figure 6. During a test before starting, the reactivation of the FC was controlled by the Agilent 6050A DC electronic load through its analog programming port in current mode, using an analog output signal of the sbRIO-9631. However, large current fluctuations that threatened the FC were present in the electronic load in the current mode. These fluctuations are due to the need of an input filter design for the electronic load, but spectroscopic models for this kind of fuel-cell are unknown and our fuel cell was damaged to make this model, therefore it was impossible to create a proper filter design. The electronic load behaved stably in the resistance mode, but this mode can not be programmed using the analog programming port for this type of electronic load. The only forms that the electronic load resistance mode can be programmed are manually or by using the GPIB port [45]. Therefore, the value of the electronic load current is sent through the ethernet port to the computer, together with the monitoring data. In the computer, it is transformed into a resistance value that is sent using the GPIB port as shown in Figure 6. Once reactivated, it will be possible to characterize the FC impedance via spectroscopy to design the input filter so that future reactivations can be performed using the electronic load in current mode. An analog output of the sbRIO-9631 was left for this purpose, also enabling its use in case of having other FC types that allow for controlling the electronic load in current mode.

Figure 6. Hardware configuration used to the reactivation of PEMFC.

The system presented in Figure 6 also can be used in the reactivation of other types of FC with more cells, with different current-levels, whether self-humidified or not. If it is necessary, it can control the temperature for reactivating the FC and is able to communicate with other systems for monitoring the main variables using advanced protocols. In addition, if it is disconnected from the computer or if there is a computer failure during its execution, the system is able to continue with the recovering of the FC, despite the faults.

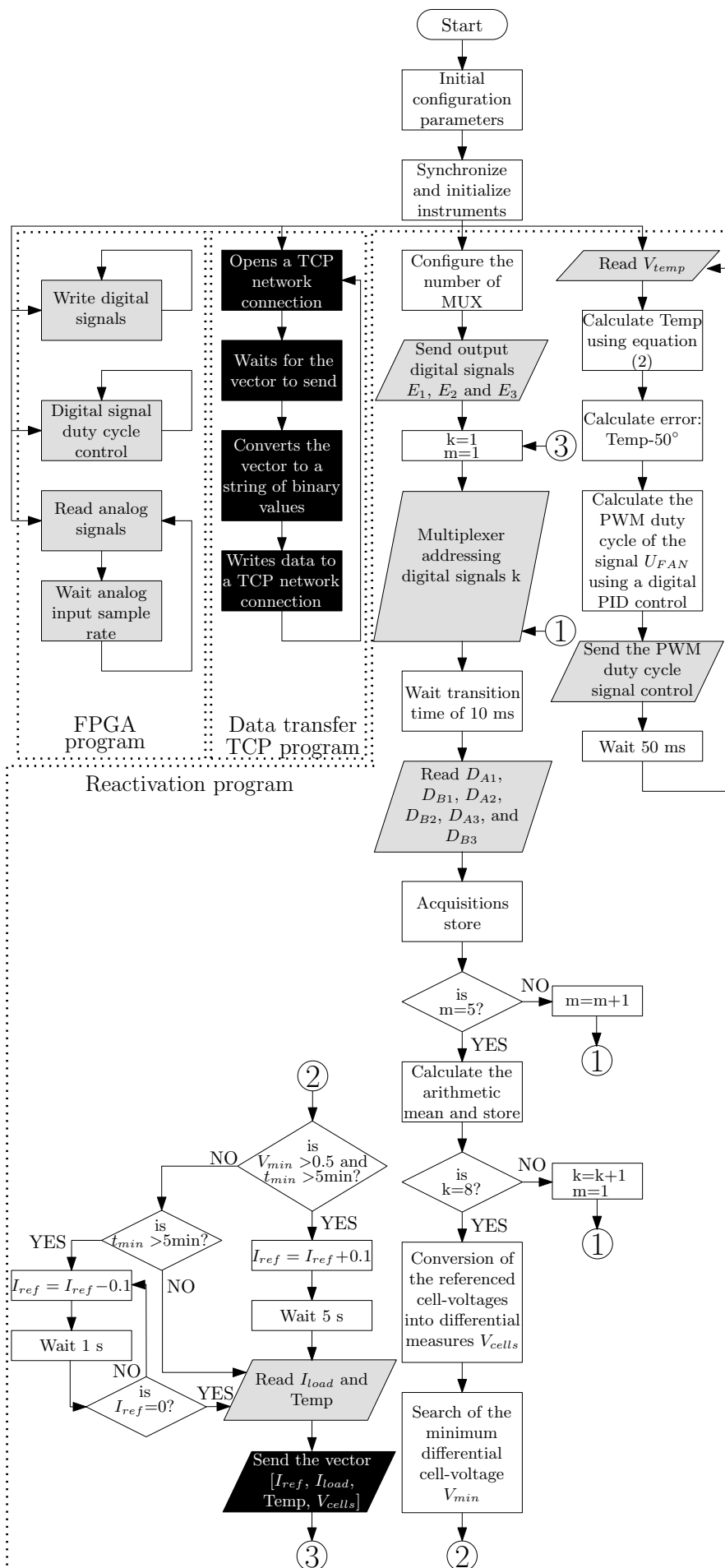
3.2. Software Architecture of the Fuel Cell Reactivation System

According to the hardware configuration shown in Figure 6, it is necessary to develop programs for the desktop computer and for the Single-Board RIO. This latter device contains the design programs for the real-time processor and for the reconfigurable FPGA. The software architecture diagram that controls the entire hardware described in the last section is illustrated in Figure 7. This subsection explains, in detail, all those programs implemented to ensure the reactivation of the FC.

Figure 7. Software architecture diagram of the FC reactivation system.

As depicted in Figure 7, the main program runs within a real-time processor that is basically responsible for executing in parallel the FC reactivation program and the transmission control protocol (TCP) communication program. The system flowchart diagram in Figure 8 has four process in parallel. The first one is responsible for FC reactivation, the second one controls the FC temperature using a digital PID, the third one writes and reads all signals connected to the reactivation system (gray rectangles), and the fourth one transmits the data to the host computer using TCP communication (black rectangles). The reactivation and the temperature control processes use the reconfigurable FPGA in order to acquire or control the different signals required for the FC reactivation, as presented in the gray rectangles in the Figure 8. All input and output signals are connected directly to the FPGA, providing low-level customization of timing, and input and output signal processing. The FPGA is connected to the embedded real-time processor via a high-speed PCI bus, as shown in Figure 7. The program of the FPGA presented in Figure 8 uses the advantage of parallel computing offered by the reconfigurable FPGA in order to acquire the analog signals, D_{A1} , D_{B1} , D_{A2} , D_{B2} , D_{A3} , D_{B3} , V_{iout} , and V_{temp} , and to control each of the digital signals, A_0 , A_1 , A_2 , E_1 , E_2 , E_3 and U_{FAN} .

Figure 8. Flowchart of the reactivation process in the Single-Board RIO.



The reactivation process has the most important function of all the designed software. The reactivation procedure is based on the methodology proposed by the fuel-cell manufacturer in order to obtain the reactivation of the stack [43], but adapting it to all the instrumentation systems designed for this purpose. A secondary objective is that it could be easily adapted to other types of PEMFCs. During the first part of this flowchart, the number of multiplexers necessary to sense the differential cell voltages within the FC according to its number of MEA's are configured using the digital output enabling signals E_1 , E_2 , and E_3 . The second part of the reactivation function presents a timed loop sequence with a period of 200 ms running in real time within the processor of the sbRIO. Inside the time-loop sequence, the truth table of the multiplexer stage, A_0, A_1, A_2 , is controlled using a repetition structure. In order to reduce the noise from the acquired signals, an arithmetic mean is calculated. Each cell-voltages is sampled five times at a frequency of 100 Hz before calculating its mean value. The next step inside the timed-loop sequence presented in Figure 8 is to convert the referenced cell-voltages into differential cell-voltages and, thus, determine the voltage per cell. This is achieved by subtracting the voltage of each cell from the cell-voltage above and then multiplying it by the gain from the resistive divider. In those cases where all the voltage cells have a voltage greater than 500 mV, the load current is increased in 100 mA and 5 s are waited to ensure the stabilization of the FC to the change of current. In the event that any of the cells voltages are smaller than 500 mV, the algorithm waits until the minimum voltage value is reached again. During each iteration of the timed-loop sequence, the FC current I_{FC} , the FC temperature T_{emp} and the cell voltages are stored and sent to the Host computer program through an ethernet port using the TCP/IP. This program successfully ensures the sending of large amounts of data, 43 variables every 200 ms. If after a maximum waiting time of 5 min the stack appears to have reached its limit, because the cell-voltage does not recover the minimum 500 mV level, it is necessary to remove the load slowly in 100 mA/s steps. Once the current is zero a human operator has to take the decision of whether to start a new iteration or not.

Finally, the host program running on the desktop computer and shown as a flowchart in Figure 9 is responsible for receiving data using TCP/IP communication. This allows the user to view and store all the reactivation information using a graphical interface and, additionally, control the electronic load through the GPIB port. As mentioned previously, the electronic load is controlled in resistive mode, therefore it was designed as a continuous function for converting the current sent by the reactivation program into a resistance value. This function is presented in Equation (3) and its characteristic curve is illustrated in Figure 10.

$$R_{load}(I_{load}) = \begin{cases} 600 - 1038 I_{load} & \text{for } I_{load} < 0.5A \\ 38.62 I_{load}^{-1.072} & \text{for } I_{load} \geq 0.5A. \end{cases} \quad (3)$$

Figure 9. Host program flowchart diagram.

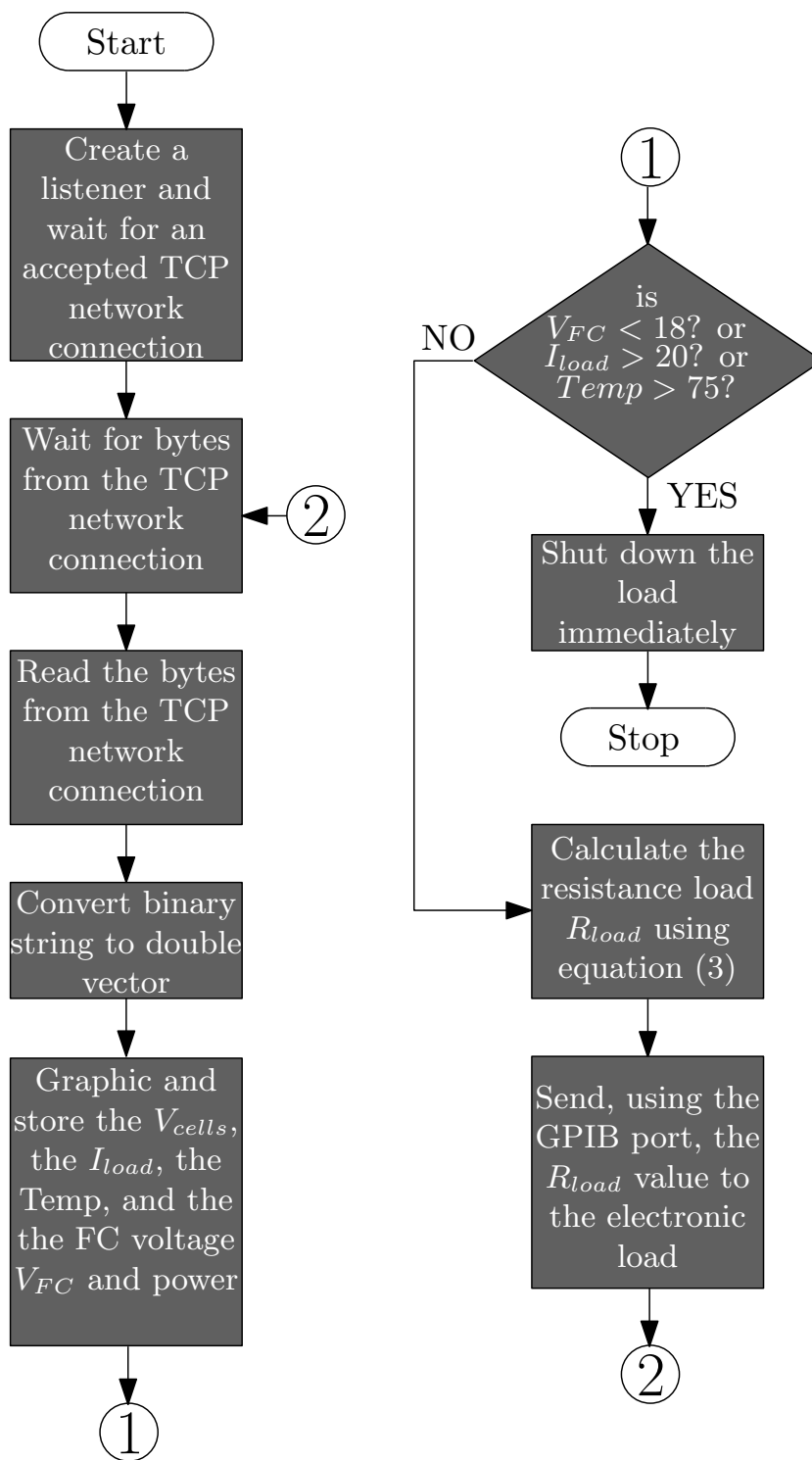
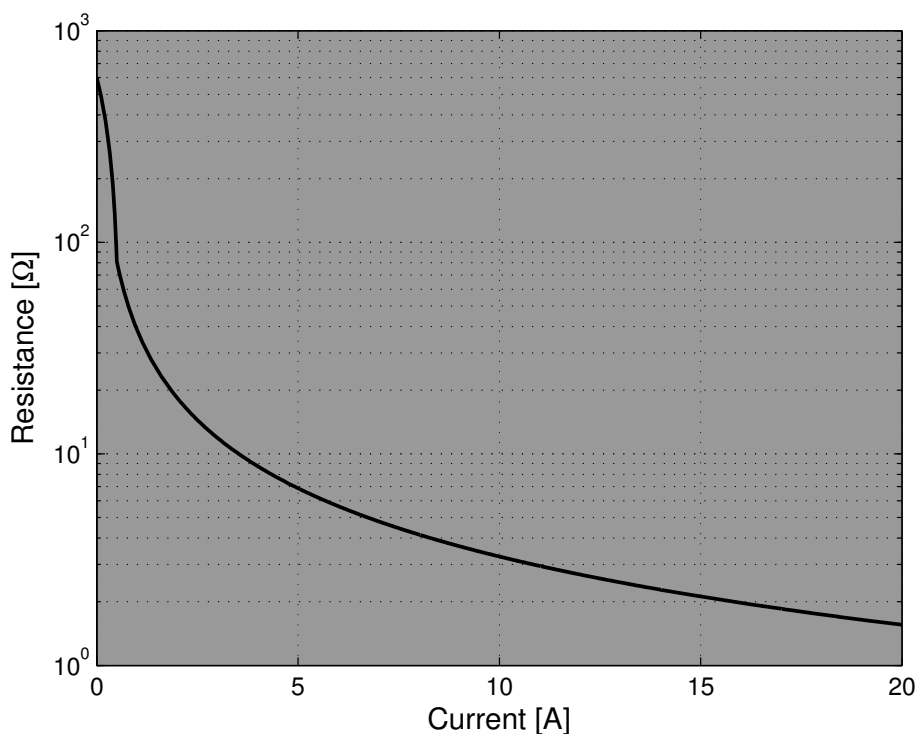


Figure 10. Characteristic curve of the electronic load in resistive mode.

4. Experimental Results

Two PC3F40 PEMFCs were reported as damaged after being stored for several years without being used. An attempt was made to reactivate one of the FCs following a manual procedure, but after reaching half its maximum rated power a sudden and permanent power drop occurred. The main consequence of the manual reactivation failure was the development of the automated reactivation system shown in Figure 11. A posterior reactivation attempt using the automatic system determined that a large number of the FC cells were always in an undervoltage condition associated to membrane damage. This first FC is still pending repair but we have been able to test the automatic system on the other twin FC. The experimental results have proved that the reactivation system has been able to reactivate the FC to a power-point of around 340 W, as shown in Figure 12. Each trace of this figure corresponds to a different cycle of the FC reactivation. A cycle ends when any of the cells voltages is under a minimum value of 500 mV for 5 min. After this undervoltage condition appears, the load is decreased slowly to 0 A as described in flowchart Figure 8 and an alarm message is shown on the computer screen. At this point a human operator has to take the decision to either initiate a new reactivation cycle or finish the procedure. In the experiments, the reactivation was ended when a seventh cycle (not shown) offered almost identical results than the sixth one. Figure 13 presents the V-I static characteristics corresponding to the reactivation experiment, in which it can be seen how the stack voltage was regaining its performance with each of the six consecutive reactivation cycles, after which an increase of more than 10 V of the FC stack's reversible potential was obtained. The depicted six cycles of the reactivation process lasted 10 h and 25 min, and had a hydrogen consumption of 1433 L at standard ambient temperature and pressure conditions (25 °C, 100 kPa). The experimental results clearly verify that the PEMFC reactivation system works properly. The system's computer interface makes it easy to use and

simplifies its reconfiguration for other models of PEMFC requiring reactivation. Since we were not able to reactivate the fuel cell using the manual procedure because the fuel cell was damaged, we can only estimate the reactivation time required by it. As an example, the last cycle of the automated procedure increased the load current from 0 A to 13.2 A in 132 steps of 100 mA. Assuming a 5 min interval for monitoring all the 40 cell voltages after each of the 132 steps, a minimum time of 11 h is required to just the last cycle. Please note that considering also the 5 more shorter cycles that were performed during all the automated reactivation, about 500 steps were applied. A rough estimation of the duration of a manual procedure with 500 current changes followed by 5-min monitoring intervals yields a minimum of 41 h and 40 min. Taking also into account the time required to regulate manually each of the 500 levels into the active load, we conclude that a comparable manual reactivation procedure takes about 4 times the duration of the automated one. A conservative estimate of the fuel required by the manual reactivation easily doubles the consumption of the automated procedure.

Figure 11. Experimental configuration used for FC reactivation: (a) PC3F40 PEMFC system; (b) PEMFC reactivation system; (c) power supply; (d) electronic load; (e) desktop computer with TCP/IP and GPIB ports; (f) fume cupboard.

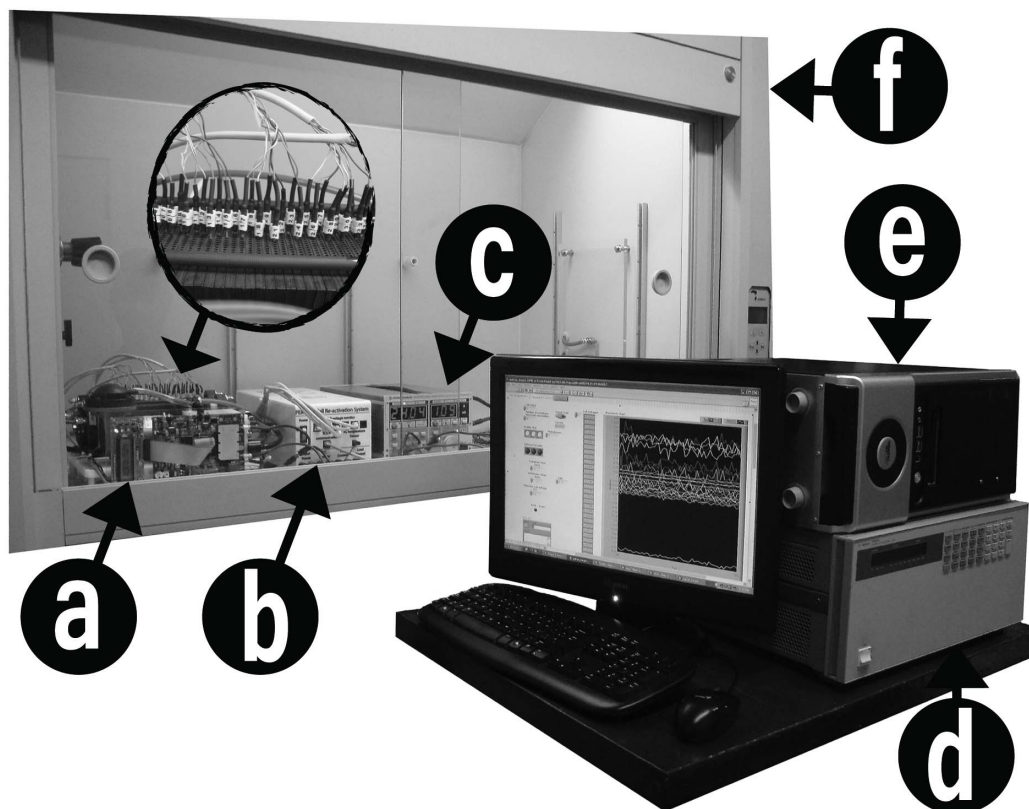


Figure 12. Fuel-cell power-current characteristic obtained following the reactivation process of flowchart Figure 8. Six reactivation cycles were required to recover a maximum power level of 340 W.

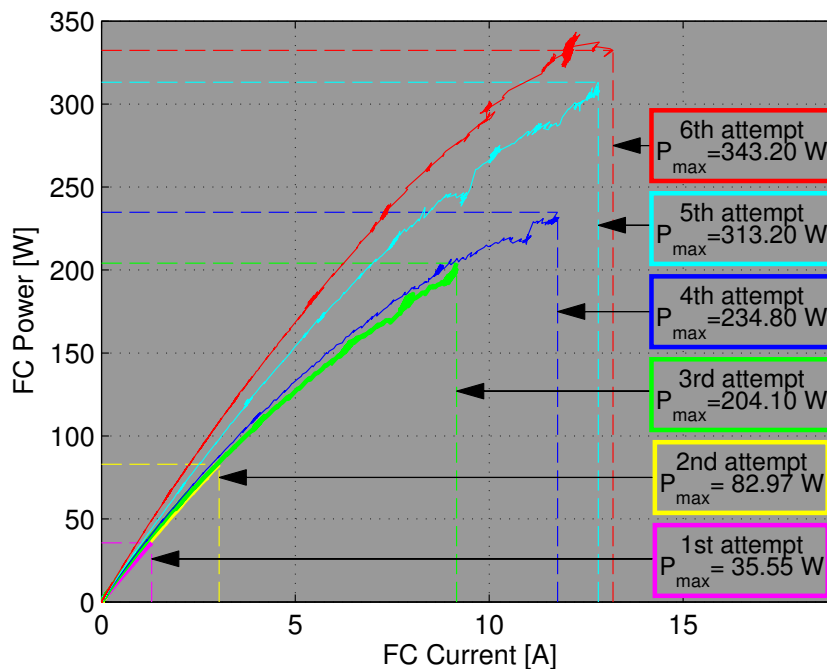
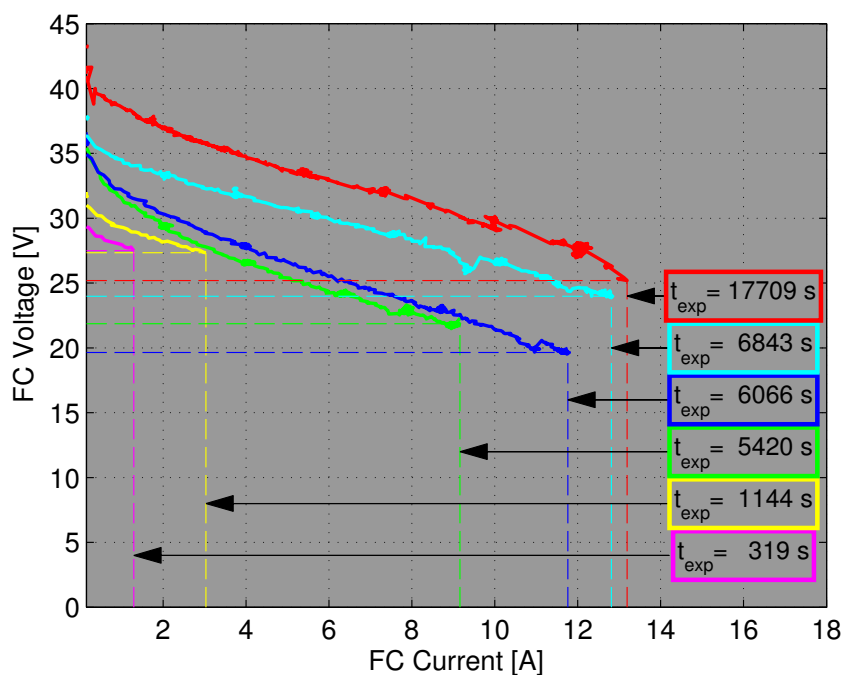


Figure 13. Fuel-cell V-I static characteristic corresponding to the reactivation of Figure 12.



5. Conclusions

After literature examination that provided no significant results, a new automated system for reactivating damaged FC has been developed and, using it, we have successfully reactivated a long

period stored PEMFC. The proposed system implementation has allowed to monitor in real-time the main FC variables and to verify in practice the validity of the reactivation procedure for a Palcan PEMFC. In comparison with the tedious and failure-prone manual reactivation procedure recommended by the manufacturer, the system regulates the fuel cell temperature and reacts almost instantaneously to the main factors that require stopping the reactivation to protect the fuel cell. It has been estimated that the duration of the automated reactivation is about four times shorter and saves half the hydrogen than using a comparable manual procedure.

Further research will address the improvement of the proposed system with an oxygen starvation detection feature that could allow the use of faster reactivation current profiles.

Acknowledgments

This work was supported by the Spanish Ministerio de Ciencia e Innovación under the projects CSD2009-00046, TEC2009-13172, DPI2010-16084 and the FPU scholarship AP2008-03305.

References

1. Larminie, J.; Dicks, A. *Fuel Cell Systems Explained*, 2nd ed.; Wiley: Weinheim, Germany, 2003.
2. Correa, J.; Farret, F.; Canha, L.; Simoes, M. An electrochemical-based fuel-cell model suitable for electrical engineering automation approach. *IEEE Trans. Ind. Electron.* **2004**, *51*, 1103–1112.
3. Pukrushpan, J.; Stefanopoulou, A.; Peng, H. Control of fuel cell breathing. *IEEE Control Syst. Mag.* **2004**, *24*, 30–46.
4. Kong, X.; Khambadkone, A. Modeling of a PEM fuel-cell stack for dynamic and steady-state operation using ANN-based submodels. *IEEE Trans. Ind. Electron.* **2009**, *56*, 4903–4914.
5. Jung, J.H.; Ahmed, S.; Enjeti, P. PEM fuel-cell stack model development for real-time simulation applications. *IEEE Trans. Ind. Electron.* **2011**, *58*, 4217–4231.
6. Aglzim, E.H.; Rouane, A.; El-Moznine, R. An electronic measurement instrumentation of the impedance of a loaded fuel cell or battery. *Sensors* **2007**, *7*, 2363–2377.
7. Ordonez, M.; Sonnaillon, M.; Quaicoe, J.; Iqbal, M. An embedded frequency response analyzer for fuel cell monitoring and characterization. *IEEE Trans. Ind. Electron.* **2010**, *57*, 1925–1934.
8. Ramos-Paja, C.; Giral, R.; Martinez-Salamero, L.; Romano, J.; Romero, A.; Spagnuolo, G. A PEM fuel-cell model featuring oxygen-excess-ratio estimation and power-electronics interaction. *IEEE Trans. Ind. Electron.* **2010**, *57*, 1914–1924.
9. Pei, P.; Yuan, X.; Gou, J.; Li, P. Dynamic response during PEM fuel cell loading-up. *Materials* **2009**, *2*, 734–748.
10. Gauchia, L.; Sanz, J. A per-unit hardware-in-the-loop simulation of a fuel cell/battery hybrid energy system. *IEEE Trans. Ind. Electron.* **2010**, *57*, 1186–1194.
11. Dhirde, A.; Dale, N.; Salehfar, H.; Mann, M.; Han, T. Equivalent electric circuit modeling and performance analysis of a PEM fuel cell stack using impedance spectroscopy. *IEEE Trans. Energy Convers.* **2010**, *25*, 778–786.
12. Chan, D.S.; Hsueh, K.L. A transient model for fuel cell cathode-water propagation behavior inside a cathode after a step potential. *Energies* **2010**, *3*, 920–939.

13. Fontes, G.; Turpin, C.; Astier, S. A large-signal and dynamic circuit model of a H_2/O_2 PEM fuel cell: Description, parameter identification, and exploitation. *IEEE Trans. Ind. Electron.* **2010**, *57*, 1874–1881.
14. Li, Q.; Chen, W.; Wang, Y.; Liu, S.; Jia, J. Parameter identification for PEM fuel-cell mechanism model based on effective informed adaptive particle swarm optimization. *IEEE Trans. Ind. Electron.* **2011**, *58*, 2410–2419.
15. Forrai, A.; Funato, H.; Yanagita, Y.; Kato, Y. Fuel-cell parameter estimation and diagnostics. *IEEE Trans. Energy Convers.* **2005**, *20*, 668–675.
16. Rathore, A.; Bhat, A.; Oruganti, R. Analysis, design and experimental results of wide range ZVS active-clamped L-L type current-fed DC/DC converter for fuel cells to utility interface. *IEEE Trans. Ind. Electron.* **2011**, *59*, 473–485 .
17. Vinnikov, D.; Roasto, I. Quasi-z-source-based isolated DC/DC converters for distributed power generation. *IEEE Trans. Ind. Electron.* **2011**, *58*, 192–201.
18. Lee, J.Y.; Jeong, Y.S.; Han, B.M. An isolated DC/DC converter using high-frequency unregulated LLC resonant converter for fuel cell applications. *IEEE Trans. Ind. Electron.* **2011**, *58*, 2926–2934.
19. Wai, R.J.; Lin, C.Y. Dual active low-frequency ripple control for clean-energy power-conditioning mechanism. *IEEE Trans. Ind. Electron.* **2011**, *58*, 5172–5185.
20. Yuan, B.; Yang, X.; Li, D.; Duan, J.; Zhai, Z.; Zeng, X. Analysis and design of a high step-up current fed multi-resonant DC-DC converter with low circulating energy and zero-current switching for all active switches. *IEEE Trans. Ind. Electron.* **2011**, *59*, 964–978 .
21. Shahin, A.; Hinaje, M.; Martin, J.P.; Pierfederici, S.; Rael, S.; Davat, B. High voltage ratio DC-DC converter for fuel-cell applications. *IEEE Trans. Ind. Electron.* **2010**, *57*, 3944–3955.
22. Zhu, X.; Li, X.; Shen, G.; Xu, D. Design of the dynamic power compensation for PEMFC distributed power system. *IEEE Trans. Ind. Electron.* **2010**, *57*, 1935–1944.
23. Leu, C.S.; Li, M.H. A novel current-fed boost converter with ripple reduction for high-voltage conversion applications. *IEEE Trans. Ind. Electron.* **2010**, *57*, 2018–2023.
24. Grötsch, M.; Mangold, M.; Kienle, A. Analysis of the coupling behavior of PEM fuel cells and DC-DC converters. *Energies* **2009**, *2*, 71–96.
25. Ramos-Paja, C.A.; Bordons, C.; Romero, A.; Giral, R.; Martinez-Salamero, L. Minimum fuel consumption strategy for PEM fuel cells. *IEEE Trans. Ind. Electron.* **2009**, *56*, 685–696.
26. Restrepo, C.; Ramos-Paja, C.; Giral, R.; Calvente, J.; Romero, A. Fuel cell emulator for oxygen excess ratio estimation on power electronics applications. *Comput. Electr. Eng.* **2012**, *38*, 926–937.
27. Pinto, F.; Vega-Leal, A. A test of HIL COTS technology for fuel cell systems emulation. *IEEE Trans. Ind. Electron.* **2010**, *57*, 1237–1244.
28. Choe, S.Y.; Ahn, J.W.; Lee, J.G.; Baek, S.H. Dynamic simulator for a PEM fuel cell system with a PWM DC/DC converter. *IEEE Trans. Energy Convers.* **2008**, *23*, 669–680.
29. Correa, J.; Farret, F.; Gomes, J.; Simoes, M. Simulation of fuel-cell stacks using a computer-controlled power rectifier with the purposes of actual high-power injection applications. *IEEE Trans. Ind. Appl.* **2003**, *39*, 1136–1142.

30. Gao, F.; Blunier, B.; Simoões, M.G.; Miraoui, A. PEM fuel cell stack modeling for real-time emulation in hardware-in-the-loop applications. *IEEE Trans. Energy Convers.* **2011**, *26*, 184–194.
31. Pukrushpan, J.T.; Stefanopoulou, A.G.; Peng, H. *Control of Fuel Cell Power Systems: Principles, Modeling, Analysis, and Feedback Design*, 1st ed.; Springer: Berlin/Heidelberg, Germany, 2004.
32. Segura, F.; Andujar, J.; Duran, E. Analog current control techniques for power control in PEM fuel-cell hybrid systems: A critical review and a practical application. *IEEE Trans. Ind. Electron.* **2011**, *58*, 1171–1184.
33. Vasallo, M.; Andujar, J.; Garcia, C.; Brey, J. A methodology for sizing backup fuel-cell/battery hybrid power systems. *IEEE Trans. Ind. Electron.* **2010**, *57*, 1964–1975.
34. Marignetti, F.; Minutillo, M.; Perna, A.; Jannelli, E. Assessment of fuel cell performance under different air stoichiometries and fuel composition. *IEEE Trans. Ind. Electron.* **2011**, *58*, 2420–2426.
35. Arce, A.; del Real, A.; Bordons, C.; Ramirez, D. Real-time implementation of a constrained MPC for efficient airflow control in a PEM fuel cell. *IEEE Trans. Ind. Electron.* **2010**, *57*, 1892–1905.
36. Suh, K.W.; Stefanopoulou, A. Performance limitations of air flow control in power-autonomous fuel cell systems. *IEEE Trans. Control Syst. Technol.* **2007**, *15*, 465–473.
37. Talj, R.; Hissel, D.; Ortega, R.; Becherif, M.; Hilairet, M. Experimental validation of a PEM fuel-cell reduced-order model and a moto-compressor higher order sliding-mode control. *IEEE Trans. Ind. Electron.* **2010**, *57*, 1906–1913.
38. *Nexa (310-0027) Power Module User's Manual, MAN5100078*; Ballard Power Systems Inc.: Burnaby, Canada, 2003.
39. Muchnic, G.; Oko, U.M.; Dannehy, C.S. Fuel Cell Stack Rejuvenation. U.S. Patent 6,558,824, 6 May 2003.
40. Adams, W.A.; Gardner, C.L.; Dunn, J.H.; Vered, R. Fuel Cell Health Management System. U.S. Patent 0,211,372 A1, 13 November 2003.
41. Adams, W.A.; Gardner, C.L.; Dunn, J.H.; Vered, R. Fuel Cell Operating Control System. WO Patent WO2003/083975 A2, 9 October 2003.
42. Adams, W.A.; Gardner, C.L.; Dunn, J.H.; Vered, R. Method And Apparatus for Rejuvenating Fuel Cells. U.S. Patent 7,038,424, 2 May 2006.
43. *Palcan Fuel Cells Sales Agreement*; Palcan Fuel Cells Ltd.: Vancouver, Canada.
44. Corporation, N.I. *NI sbRIO-961x/963x/964x and NI sbRIO-9612XT/9632XT/9642XT User Guide*; National Instruments Corporation: Austin, TX, USA.
45. *Operating Manual, Electronic Load Mainframes Models 6050A and 6051A*; Agilent Technologies: Beijing, China, 1997.